

The development of a bioreactor to perfuse radially-confined hydrogel constructs: Design and characterization of mass transport properties

Joshua O. Eniwumide*, David A. Lee and Dan L. Bader

Medical Engineering Division and IRC in Biomedical Materials, School of Engineering and Materials Science, Queen Mary University of London, Mile End Road, London, UK

Received 20 April 2009

Accepted in revised form 21 September 2009

Abstract. Limitations to nutrient transport provide a challenge to the development of 3D tissue-engineered constructs. A heterogeneous distribution of viable cells and functional matrix within the developing tissue is a common consequence. In the present study, a bioreactor was developed to perfuse fluid through cylindrical agarose constructs. The transport and distribution of dextran molecules (FD-4, FD-500, FD-2000) within the agarose was visualized in order to determine the bioreactors effectiveness for transport enhancement. By 24 h, the perfusion bioreactor achieved 529%, 395% and 294% higher concentrations of FD-4, FD-500 and FD-2000, respectively, than those solely due to diffusion. Of particular interest was the effectiveness of the bioreactor to transport molecules to the central region of the constructs. In this respect, the perfusion bioreactor was found to increase transportation of FD-4, FD-500 and FD-2000 by 30%, 291% and 222% over that of diffusion. Articular chondrocytes were cultured and perfused using the bioreactor. The improved molecular transport achieved led to an average 75% and 1340% increase of DNA and sulphated GAG, respectively at 20 days. More significantly was the 106% and 1603% increase of DNA and GAG, respectively, achieved at the central core of the 3D constructs.

Keywords: Bioreactors, tissue engineering, molecular transport, fluid flow, perfusion chondrocytes

1. Introduction

Surgical interventions, tissue grafts and cell transplantations are well-established strategies for treating diseased, hereditarily abnormal, or damaged tissues [2,3,26,36,37,41]. At most, these solutions offer structural replacement, with no immunological rejection. Tissue engineering aims to provide biologically-led solutions that will be compatible; integrate completely with host tissue and restore long term function to treat a variety of clinical conditions. This includes the restoration of cartilage function following damage caused by trauma or pathology. Key activities in this approach are the obtaining and expanding of cells [22,40,45], and the development of 3D scaffolds, which carry the cells [13,15,19,20].

* Address for correspondence: Dr. Joshua Eniwumide, Marie Curie Research Fellow, Charité – Universitätsmedizin Berlin, Centrum für Muskuloskeletale Chirurgie, Forum 4 Psf 24, Augustenburger Platz 1, D-13353 Berlin, Germany. Tel.: +49 30 450 559087; Fax: +49 30 450 559969; E-mail: joshua.eniwumide@charite.de.

Moreover, the scaffolds function to retain the cells at the defect site, allowing them to multiply and synthesize the extracellular matrix to provide mechanical competence.

To date, many cartilage tissue-engineering strategies encounter a significant technical challenge when chondrocytes are cultured for prolonged periods in a 3D environment. This is defined by the loss of cellular viability in the central region of the construct. Diffusion, the mechanism that supplies oxygen, and soluble nutrients, and removes metabolic waste, is often inadequate when constructs are maintained under standard static culture conditions [4,25,28]. Consequently, cell-seeded scaffolds thicker than 1 mm generally consist of a viable periphery, encasing a hypoxic, necrotic centre [17,31,39]. Moreover, glycosaminoglycan (GAG) production by chondrocytes and mineralized matrix deposition by osteoblasts have been reported to be curtailed approximately 400 μm and 240 μm from the surface, respectively [21,31,39].

To address the limitation to nutrient transport, bioreactor systems have been utilized with an aim to improve nutrient delivery to all regions of tissue-engineered constructs. Both stirred-flask and rotating-wall vessel bioreactors induce medium flow around constructs, resulting in an enhanced GAG synthesis by chondrocytes in macroporous 3D constructs [1,8,11,14,29,31,38,42]. However spatial heterogeneity remains. Direct perfusion bioreactors provide fluid flow through the construct to augment the delivery of nutrients to the centre of 3D constructs [6,7,32,33,47,48].

The present study describes a perfusion bioreactor that has been designed specifically to generate dynamic fluid flow through a 3D agarose construct, which is used extensively as a model system in cartilage tissue engineering. This paper provides an initial characterization of the bioreactor system using cell-seeded agarose constructs, of physiologically relevant dimensions. A fluorescence-based method was used to assess spatially the enhancement of molecular transport. Furthermore, its ability to promote cellular proliferation and matrix synthesis was demonstrated at a nutritionally-demanding cell concentration.

2. Materials and methods

2.1. Bioreactor design

The perfusion bioreactor was designed to confine a cylindrical construct, 10 mm diameter and 3 mm thickness, within a chamber. This strategy was adopted in order to eliminate fluid flow around the construct and maximize the molecular transport through the constructs. The major components of the bioreactor were made from medical grade stainless steel (316L). In addition to its biocompatibility, the metal could be repeatedly autoclaved, which is a very effective, relatively fast and cheap method of sterilisation. Each bioreactor unit was designed to maintain one specimen, rather than several specimens (which would have been more efficient) because the individualized chambers enabled sampling of constructs for subsequent analysis without disrupting other ongoing experiments.

The bioreactor system further incorporates a syringe pump, medium reservoir and delivery tubes (Table 1).

2.1.1. Perfusion chamber

The perfusion chamber, made up of three pieces ($\text{CP}_{1,2,3}$; (Fig. 1a–c)), and is symmetrical about the central disc (CP_2) that has a diameter of 50.8 mm and incorporates four holes. Three of these holes are 5 mm in diameter and allow passage of the screws used while assembling the bioreactor components. The fourth hole is located centrally, having a 10 mm bore and a threaded inner wall. It is in this central hole that the agarose is gelled and maintained during operation. Both the top (CP_1) and the bottom

Table 1

Major components of the confined perfusion bioreactor, their materials and respective sources

Components	Materials	Source
Flow chamber	Medical grade Stainless steel	Smith & Sons, London, UK
Screws	Stainless steel	Smith & Sons, London, UK
O-rings	Rubber	
Piping	Silicone	Watson Marlow Pumps, UK
* 50 ml syringes	Polypropylene	PLASTIPAK [®] BD [®]
Porous filter	Polypropylene	Amersham Biosciences, UK

Note: * Single use component. All other components may be heat-sterilized at 126°C and 100 kPa to allow repeat use.

pieces (CP₃) have an inlet and outlet port, respectively, each with a 1.5 mm bore. These open to a dome-like space with a depth and diameter of 2.4 mm and 11.5 mm, respectively. The dome opens up into a cylindrical space that has a 15.5 mm diameter and a 2 mm depth and is snap-sealed with the porous plastic filter. Encasing the filter in CP₁ and CP₃ is a rubber O-ring (CP_O), having a 10.2 mm radius. These are locked tightly into a machined circular groove with a 1.3 mm depth. The O-rings on both CP₁ and CP₃ protrude slightly to prevent fluid leakage. The three peripheral holes in CP₃ are threaded, to permit screw fastening during assembly (Fig. 1d). The porous polypropylene filters (15 mm diameter, 2 mm thickness, pore size and porosity of 50–150 µm and 70%, respectively; Sigma-Aldrich, St. Louis, MO, USA) were incorporated into both CP₁ and CP₃, where they supported the agarose constructs.

2.1.2. Syringe pump, syringe and delivery tubing

A commercially available, programmable 10-channel syringe pump (Harvard Apparatus PHD 71-2109 VHP) was used to deliver fluid to the perfusion chamber. The pump operates using a screw-driven micro stepper, which eliminates flow pulsation. By employing a multiple syringe rack, simultaneous perfusion of several bioreactors was possible. Sixty ml plastic syringes (BD Plastipak[™], Madrid, Spain) were mounted on the syringe pump and acted as a reservoir for the perfused fluid. The fluid was delivered to the perfusion chamber via semi-permeable silicone tubes (Watson Marlow Pumps, UK). The tubes are durable, could be readily autoclaved and are oxygen-permeable. Thus, the tubes served the purpose of oxygenation and CO₂ delivery to the culture media to ensure viability and proliferation of the cells in culture.

2.1.3. Diffusion

FITC-dextran powder was dissolved in phosphate buffered saline (PBS: Sigma-Aldrich, UK) at a concentration of 0.01% (wt/vol). Solutions were prepared with dextran of three different molecular weights (4, 500 and 2,000 kDa, denoted by FD-4, FD-500 and FD-2000, Sigma-Aldrich, UK). Ultra-low gelling temperature agarose powder was dissolved by autoclaving in Earle's Balanced Salt Solution (EBSS) to yield a concentration of 4% (wt/vol). The resultant agarose solution was cast into a mould, containing 10 mm × 3 mm holes, with the bottom supported by a glass slide. A second glass slide was placed on the molten agarose and tightly secured using sterile clips to enable gel solidification without leakage (Fig. 2a). Solidification was achieved by maintaining the covered mould at 4°C for 10 min. Once the agarose had gelled, the supporting glass slides were removed from both surfaces and the agarose constructs were extracted and transferred into falcon tubes containing 10 ml of FITC-dextran solutions. The specimens were divided into four groups. The three experimental groups were incubated for up to 24 h at 21 ± 1°C in 0.01% (wt/vol) solutions of; FD-4, FD-500 or FD-2000 in PBS. As a control, the fourth

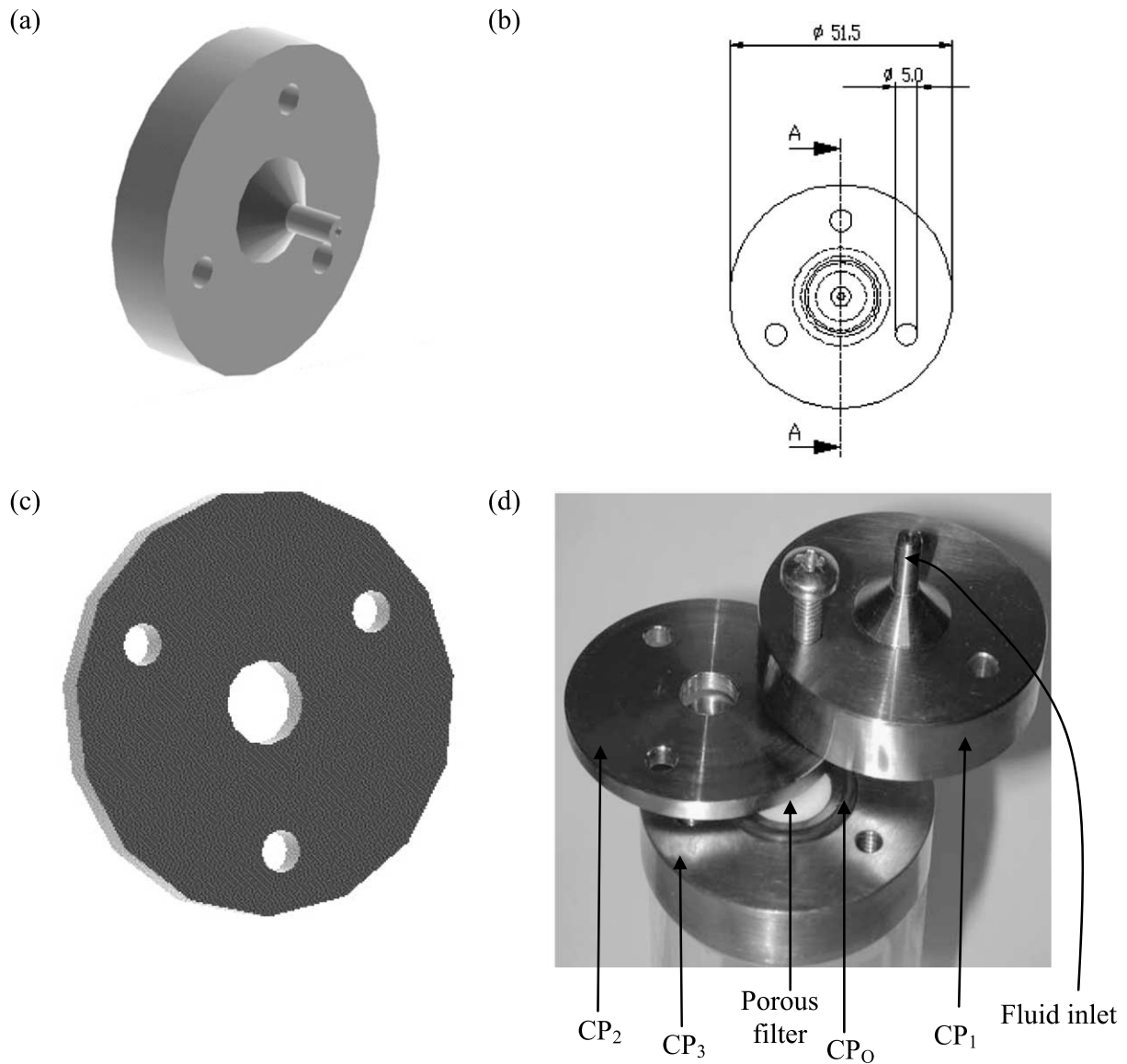


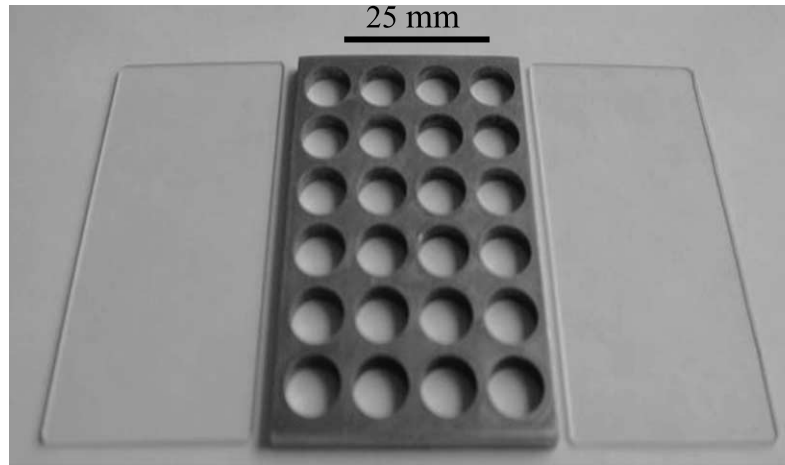
Fig. 1. The perfusion bioreactor. (a) The major components of the perfusion bioreactor, namely CP₁ and CP₃, which have similar dimensions (b). (c) The central disc CP₂. This has a 10 mm × 3 mm hole machined at its centre. Inside of which, the molten specimen is gelled. (d) Assembling of the bioreactor.

group was incubated for 24 h in PBS alone, at $21 \pm 1^\circ\text{C}$. These provided a baseline for fluorescent intensity in the absence of the fluorescein–dextran molecules. These experimental groups are termed the diffusion group. Three samples were removed from each batch for analysis at 1, 2, 4, 8 and 24 h in order to measure the temporal diffusion of dextran molecules.

2.1.4. Perfusion

For perfusion experiments, a 4% (wt/vol) agarose solution was prepared as described above. The molten gel was transferred into the central hole of CP₂ of the bioreactor with the bottom supported by a

(a)



(b)

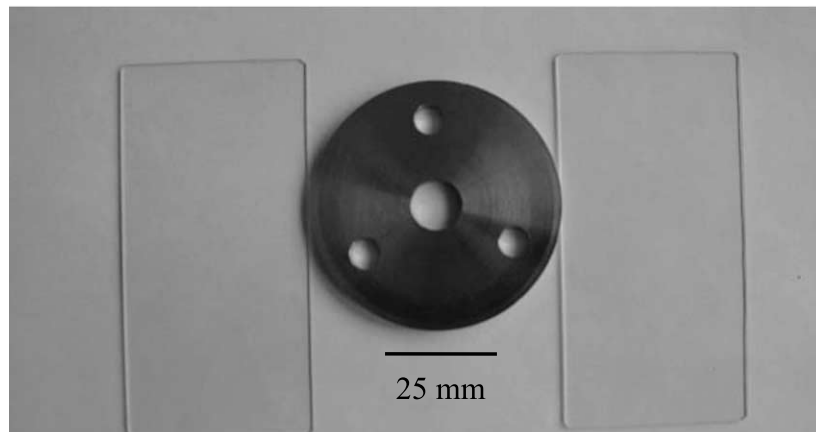


Fig. 2. Stainless steel moulds and the glass slides used for gelling agarose constructs in (a) diffusion experiments and (b) CP₂ used for specimens to be perfused. Each hole was 10 mm in diameter and 3 mm deep.

glass slide. A second glass slide was placed on the molten agarose and tightly secured using sterile clips to enable gel solidification without leakage (Fig. 2b), and incubated for 10 min at 4°C. CP₂, containing the agarose construct, was subsequently aligned and assembled with CP₁, CP₃, with their associated O-rings and porous supports. The perfusion chambers were connected to an individual syringe via silicone tubes. Following assembly, the entire system was primed with one of the three dextran solutions. The samples were incubated in the bioreactors for up to 24 h and representative samples were analysed at 1, 2, 4, 8 and 24 h. Perfusion of the FITC-dextran solutions was performed at $21 \pm 1^\circ\text{C}$, and at a volumetric flow rate of 1.00 ml/h for up to 24 h. Given that the nominal surface area of the agarose constructs was 0.79 cm^2 ; this volumetric flow rate yields a mean flow velocity of 1.27 mm/h. In a separate experiment, constructs were maintained inside the bioreactor system but without fluid flow.

2.1.5. Data analysis

A protocol was developed for measuring the transport of dextran molecules either by diffusion or perfusion, and to incorporate the visualization of the molecular distribution within the 3D constructs. This protocol, which involved the bisecting of the agarose constructs, and obtaining a montage of fluorescent values across the 3 mm thick longitudinal surface, is reviewed briefly. Representative constructs were harvested, bisected in the longitudinal plane into two hemi-cylinders using a sharp scalpel (Fig. 3a). These were transferred onto a microscope coverslip, with the cut surface exposed for imaging, and mounted onto the stage of an inverted fluorescence microscope (Fig. 3b). A small volume of fluid was pipetted onto the specimen to maintain its hydration during imaging. Fluorescent scans were made vertically across the 3 mm section using a $\times 20$ Plan *Apo* objective lens, with a numerical aperture of 1.4, and at a laser excitation wavelength of 488 nm. A series of images were captured at an emission wavelength of 535 nm across the mid-plane longitudinal surface of the agarose construct. The motorized stage of the microscope was used to move across the specimen and obtain a montage (Fig. 4a) of images across the 3 mm thickness. From the acquired images, measurements of grey pixel, corresponding to the fluorescent intensities were made systematically in a direction parallel to scanning direction (along the white line across the micrographs in Fig. 4a).

Fluorescent profiles across the mid-plane longitudinal sections were exported to an Excel spreadsheet as a plot of fluorescence versus pixel number (Fig. 4b). Each pixel number was converted into distance from the construct surface, taking into account the microscope settings, camera binning and objective magnification as indicated by the microscope manufacturer. From these conversions, graphs of fluorescence (y-axis) as a function of distance from the top surface of the construct were generated. These were subsequently normalized, such that 0 and 1 represented the top and bottom surfaces, respectively (Fig. 4c).

By examining Fig. 4b, it may be observed that the individual micrographs and fluorescent profiles at either edges of the montage begin with regions of relatively low fluorescence. However the intensity values rise sharply, from average values of 110–200 (and higher in the case of perfused constructs). The positions of this sudden increase represent the edge of the specimens, and values prior to and after these were omitted from subsequent calculations. The distance between the two edges were those normalized from 0 to 1, representing the upper and lower surfaces of the specimens, respectively. The arbitrary grey values were converted into an intensity profile in the following manner: Table 2 illustrates the method used to convert the fluorescent data obtained from the montage into a fluorescence-distance data:

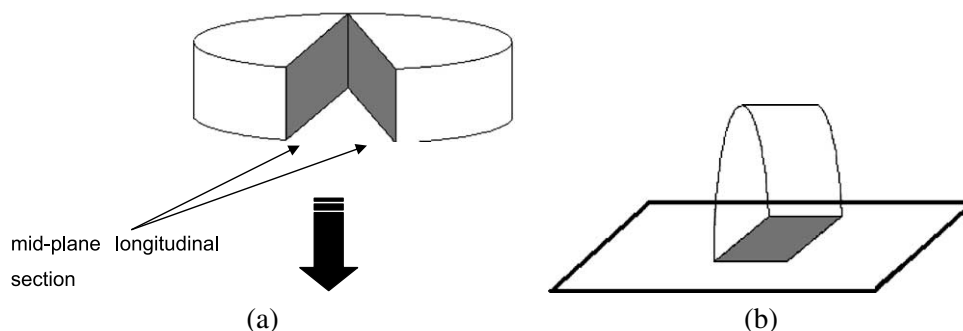


Fig. 3. (a) Each construct was bisected to expose its mid-plane longitudinal section (shaded grey for imaging). (b) The specimen was placed on a microscope slide and mounted on an inverted-stage fluorescent microscope.

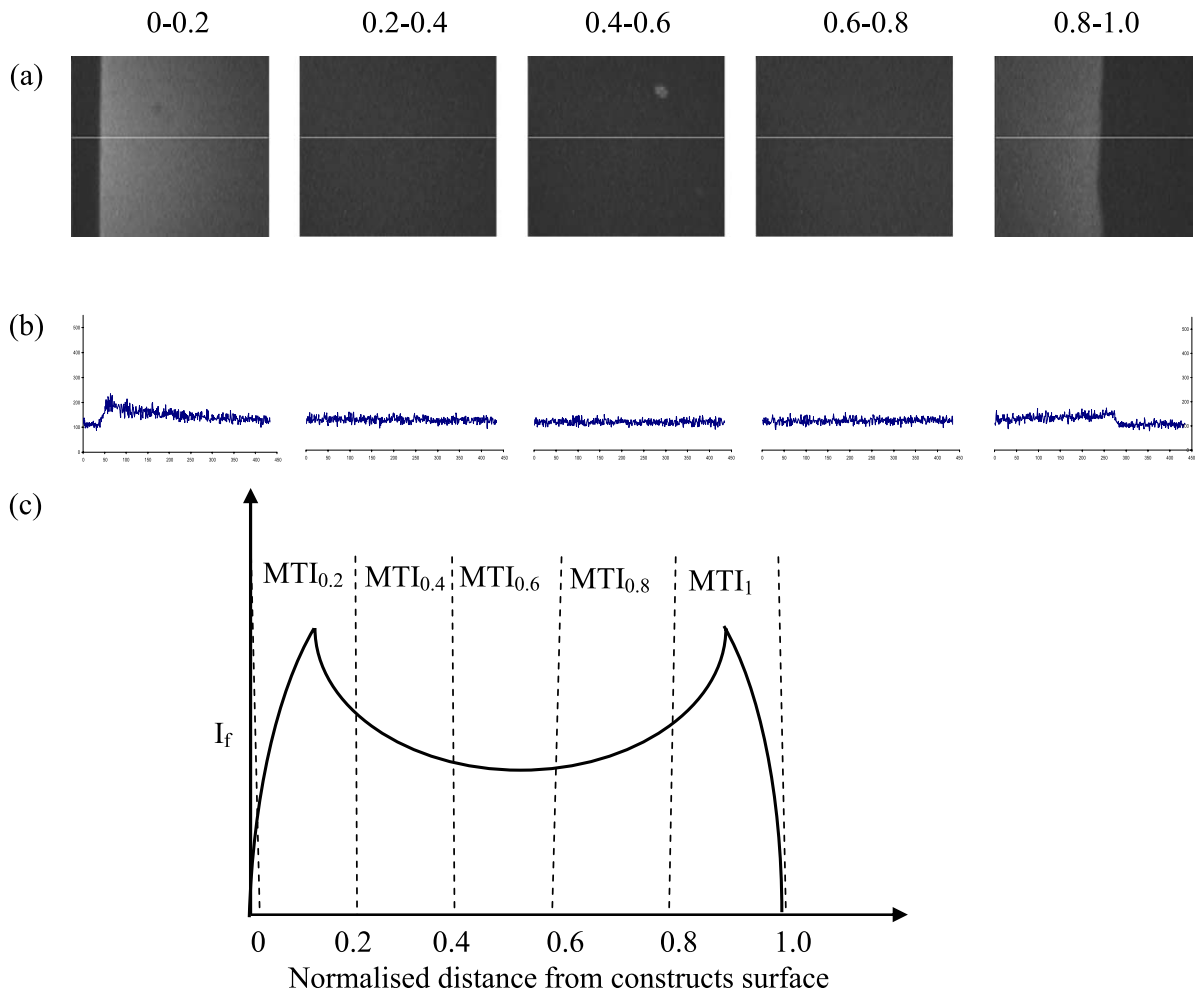


Fig. 4. Montage of fluorescent intensities obtained systematically across the 3 mm mid-plane longitudinal section of the agarose constructs. The white lines running across each micrograph (a) were the region where fluorescence was profiled. Values measured using these lines were produced in the graphs (b), which show fluorescent values with respect to distance. The combined graphs, from one surface to the other were divided into 5 parts, and normalized with respect to distance across the construct depth (c).

- Column A contains the pixel number while column B contains the fluorescent values (Table 2).
- Column C is the pixel size, which was calculated as directed by the microscopes manufacturer, taking into account the objective lens used and the apparatus settings.
- Column D has the integrated fluorescent values across the specimen plane of interest, from which E, giving the cumulative values are derived. Therefore, the last figure of column E gives an integration of the entire area that was imaged, from point 0 to point 1 of the specimen ($tMTI$).

Each full-depth profile of fluorescent data was divided into 5 equal segments along the 3 mm longitudinal axis. From this, a Mass Transport Index (MTI) for each of the 5 regions was derived using Eq. (1).

Table 2

The steps involved in converting the fluorescent values profiled across the agarose constructs into comparable parameters for determining fluorescent intensity and dispersion within the 3D constructs

A	B	C	D	E
Pixel number	Fluorescent value (example)	Pixel size (μm)		Area under curve
1	110	2.04	$(B_1 * 2.04) = 224.4$	D_1
2	204	2.04	$(B_2 * 2.04) = 416.16$	$D_1 + D_2$
3	211	2.04	$(B_3 * 2.04) = 430.44$	$D_1 + D_2 + D_3$
n	FV	2.04	$(B_{FV} * 2.04) = 2.04_{FV}$	$D_1 + D_2 + D_3 + \dots + D_{FI}$

Note: * 2.04 is the numerical factor used to convert pixel number to distance (in μm) as directed by the microscope's manufacturer, taking into account the objective lens used and the apparatus settings.

These were defined as the amount of fluorescence within each of the 5 segments:

$$MTI = \sum_{n=0}^{n=0.2} \delta[I_n], \quad (1)$$

where I is the fluorescent intensity at position δ . This is the incremental distance, corresponding to the pixel size (approximately $0.2 \mu\text{m}$); n is the depth at which MTI is calculated, for example, $MTI_{0.2}$ and MTI_1 can be calculated as follows:

$$MTI_{0.2} = \sum_{n=0}^{n=0.2} \delta[I_n + I_2 + I_3 + \dots + I_n] \quad (2)$$

and

$$MTI_{1.0} = \sum_{n=0.8}^{n=1.0} \delta[I_n + I_2 + I_3 + \dots + I_n]. \quad (3)$$

The values indicated the amount of dextran molecules within the 5 segments of the constructs, and hence their dispersion across the 3 mm depth. The sum of the 5 MTI values represents the total fluorescence, and is therefore indicative of the extent of dextran transportation into the agarose constructs, the equation for which is given by:

$$tMTI = \sum_{n=0}^{n=1.0} MTI. \quad (4)$$

2.1.6. Field curvature aberration

The effect of field curvature was observed in the present study. This aberration occurs naturally due to the curvature of the objective lens. In photomicrography, the aberration results in the centre of the field of view being in a different focal plane than that at the edge. Thus, the image appears sharp at either the centre, or at the edges of the field of view, and not simultaneously at both positions. In the present study, the aberration resulted in overestimated fluorescent intensity at the centre of the field of view. Moreover, this evolved into a series of peaks in a montage of fluorescent profiles across the constructs thickness (Fig. 5a).

The lens aberration was addressed by applying the *flat-field correction* technique as directed by the microscope manufacturer. This was conducted prior to the quantitative analysis, and involved taking a

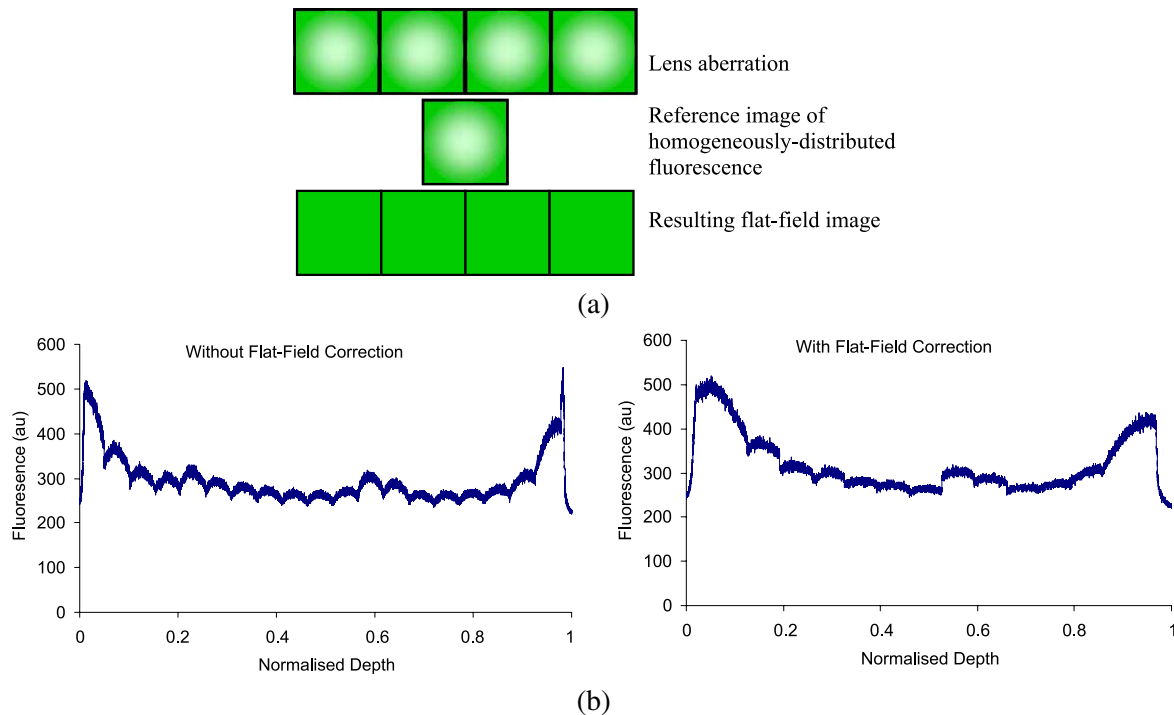


Fig. 5. (a) Schematic, showing effects of field-curvature aberration on a fluorescent profile across an agarose construct and its correction with the use of a reference image. (b) The resulting fluorescence profile without (left) and with (right) flat-field correction.

fluorescent image, with a homogenous fluorescence profile, which is used as a reference image. This image is then compared with the fluorescent profiles obtained to deduce the true fluorescent values at the centre of each field of view (Fig. 5b).

2.2. Chondrocyte isolation and culture

Full-depth slices of cartilage were removed from the metacarpophalangeal joints of 18-month-old steers. The cartilage slices were incubated at 37°C on rollers for 1 h in culture media, plus 700 U/ml pronase (BDH, Poole, UK). The culture media contained Dulbecco's modified Eagle's medium (DMEM) supplemented with 16% (v/v) foetal calf serum (FCS), 2 µM/ml L-glutamine, 5 µg/ml penicillin, 5 mg/ml streptomycin, 20 mM HEPES buffer and 0.85 mM L-ascorbic acid (all from Sigma Chemical Co., Poole, UK). The slices were further incubated for up to 18 h at 37°C in the culture media plus 100 units/ml of the enzyme, type II collagenase (Sigma). The lysates were passed through a 70 µm pore-size cell sieve (Falcon Ltd., Oxford, UK) and were washed three times in DMEM plus 16% FCS.

The total cell number and percentage viability were quantified, using a well-established trypan blue method. The cells were subsequently seeded in the appropriate volume of medium and molten agarose to attain a cell concentration of 20×10^6 cells per ml of 4% (wt/vol) agarose. The agarose/chondrocyte suspensions were cast into moulds and gelled at 4°C, either in the central whole of CP₂ (Fig. 2b) of the bioreactor, or in a separate mould (Fig. 2a). The latter group were released from the mould, and cultured inside Petri dishes, serving as control groups.

The sterilised components of the bioreactors and the plastic syringe were transferred to a sterile laminar flow cabinet and assembled with the solidified cell/agarose constructs incorporated into the perfusion chambers. The syringe and the silicone tubing were connected and primed with the culture medium, to eliminate air bubbles. Each syringe, fitted to the syringe pump, and the bioreactors were transferred to a CO₂ incubator. Culture media was perfused at the flow rate of 0.47 ml/h. At this flow rate, 22.6 or 33.9 ml of medium was perfused within a 48 or 72 h period. At these times, the syringe was changed and fresh medium was supplied. For a direct comparison, the free-swelling cultures were maintained in either 22.6 or 33.9 ml of medium per construct, for up to 48 or 72 h, respectively, prior to being replenished. The constructs were cultured for up to 20 days.

2.3. *Measuring DNA and GAG*

Chondrocyte-seeded agarose constructs were sampled after 1, 6, 10 and 20 days. These were incubated at 60°C in 1 ml of phosphate PBS, supplemented with 10 mM ethylenediaminetetraacetic acid (EDTA, BDH Chemicals) and 10 mM L-cysteine hydrochloride (BDH Chemicals) until molten. The suspensions were cooled to 37°C and incubated overnight with 10 µl of agarase at a concentration of 1000 units/ml (Sigma Chemical Co., UK) and 5 µl of papain at a concentration of 560 units/ml (Sigma Chemical Co., UK). Following this, the mixture was incubated for a further 60 min at 60°C.

The solutions were assayed in triplicate for both sulphated glycosaminoglycan (GAG), and DNA content using the dimethyl-methylene blue (DMB) assay [9] and an adaptation of a well established method based on a commercially available bisbenzimidazole dye, Hoechst 33258 (Sigma Chemical Co., UK) [23], respectively.

2.4. *Sampling the central core*

The central core of the constructs was defined as the centre 4 mm diameter by 1 mm thick regions of the original 10 mm diameter × 3 mm thick cylindrical construct. These samples were obtained using a cork borer, with a 4 mm internal diameter, and a size 11 scalpel blade, as indicated schematically in Fig. 6. The borer was positioned centrally on the top surface of the cultured 10 mm diameter agarose constructs. The coring yielded a full thickness cylinder, with 4 mm diameter.

This cylinder was then divided into three 4 mm × 1 mm constructs. The central core was enzymatically digested and assayed biochemically for GAG and DNA concentrations. These cylindrical sub-cores were extracted from constructs that had been cultured for 1, 6, 10 and 20 days in free-swelling conditions or perfused with the bioreactor.

2.5. *Statistical analysis*

Comparisons of *t*MTI values were made between diffusion and perfusion, using Student *t*-test ($p < 0.05$). Similarly, all DNA and GAG data were analysed from 6 days onwards, direct comparisons being made between the perfused and the free-swelling cultures.

3. Results

3.1. *Diffusion within agarose constructs*

The MTI values of dextran molecules for the diffusion experiments are presented in Fig. 7a–c. Values for the groups incubated without FITC-dextran molecules are also indicated (Fig. 7d). It is clear that the

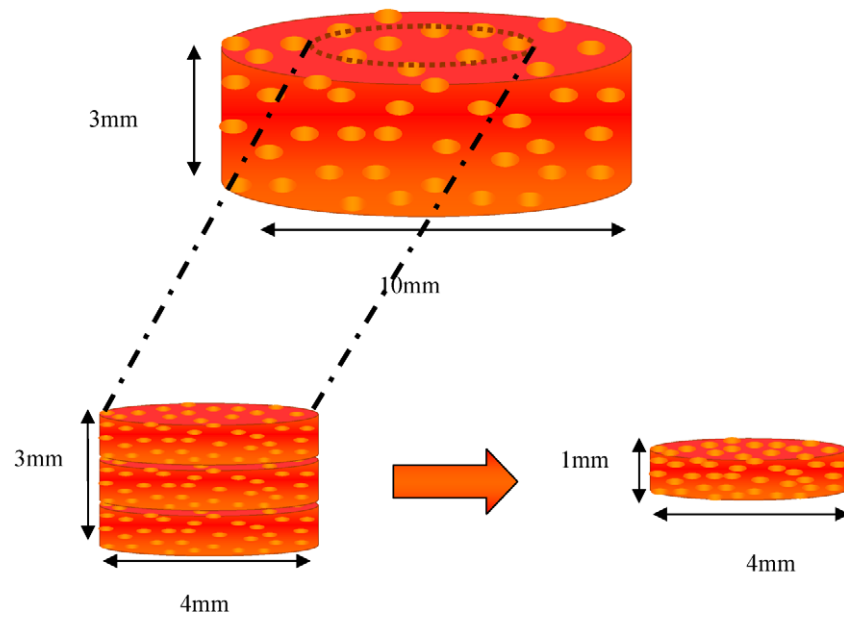


Fig. 6. Schematic diagrams, illustrating the steps involved in obtaining a cylindrical sample from the central region of the chondrocyte-seeded agarose constructs.

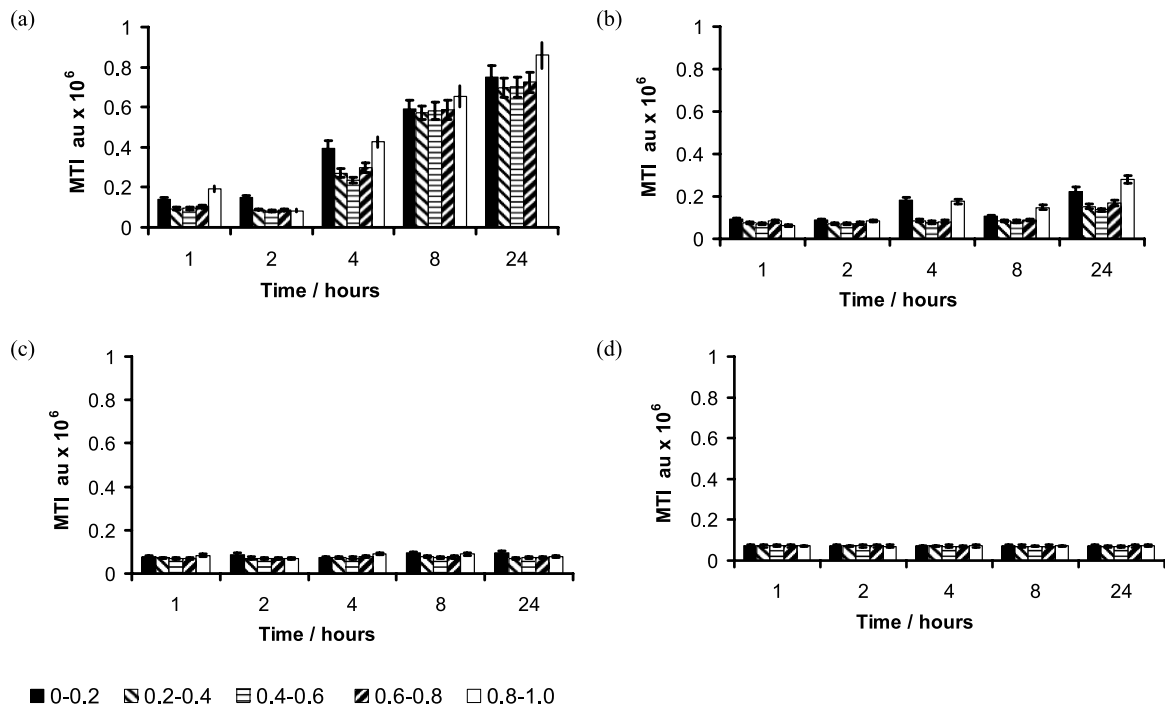


Fig. 7. Histograms illustrating the average MTI of FITC-dextran in five equal sections of the 3 mm thick agarose constructs in the free-swelling diffusion. Molecules of size (a) 4 kDa (FD-4), (b) 500 kDa (FD-500) and (c) 2,000 kDa (FD-2000) were used. The control group (d) illustrates MTI in the absence of FITC molecules. The fluorescence is presented as arbitrary units (au) and the data represents mean \pm standard deviation of 4–6 replicates.

MTI values were highest for the FD-4 molecules (Fig. 7a). Additionally, for FD-4 and FD-500, MTI values at the edge of the construct (at depths 0–0.2 and 0.8–1.0) were considerably higher than those at their centre. However, by 24 h, the corresponding differences between these regions were considerably smaller, with their differences reduced to 7.2%. For FD-2000, there were negligible differences in MTI values across the construct and with respect to incubation time (Fig. 7c). Moreover, very small differences were noted between the fluorescence of FD-2000 and the control group, which had not been incubated with the fluorescent molecules (Fig. 7d).

3.2. The influence of fluid convection on molecular transport

The temporal diffusion of the three molecular weight dextran molecules into the agarose construct in the confined bioreactor, in the absence of fluid flow, is illustrated in Fig. 8. In a manner similar to that in the diffusion experiments, the spatial and temporal distributions of the diffused molecules within the confined bioreactor were more pronounced with FD-4 and FD-500. A comparison of Fig. 7 with Fig. 8 clearly shows that, for all three molecular weight dextrans, fluorescence associated with diffusion was higher than that within the bioreactor without fluid flow. This suggests that the immediate environment

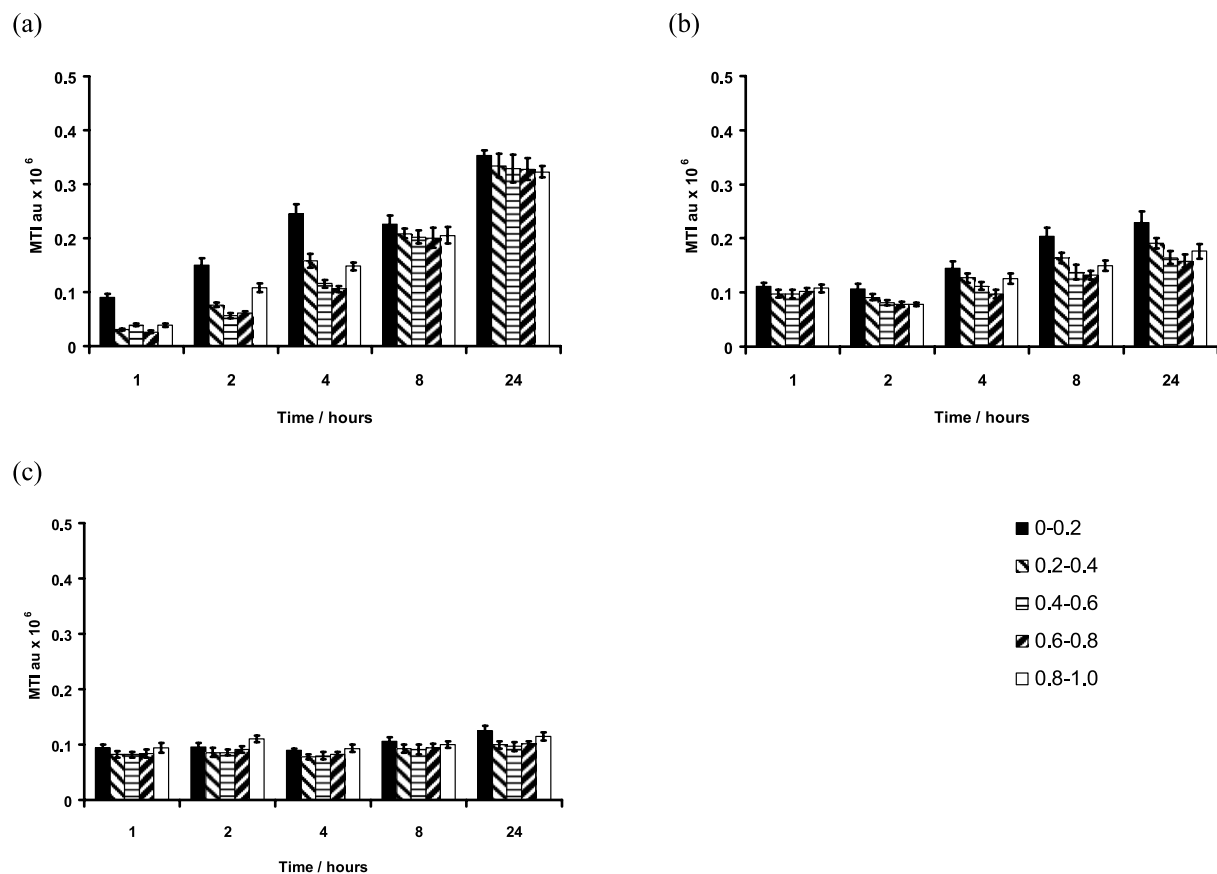


Fig. 8. Histograms illustrating the average MTI of FITC-dextran in five equal sections of the 3 mm thick agarose constructs in the confined bioreactor, without flow. Molecules of size (a) 4 kDa (FD-4), (b) 500 kDa (FD-500) and (c) 2,000 kDa (FD-2000). Data represents mean \pm standard deviation of 4–6 replicates.

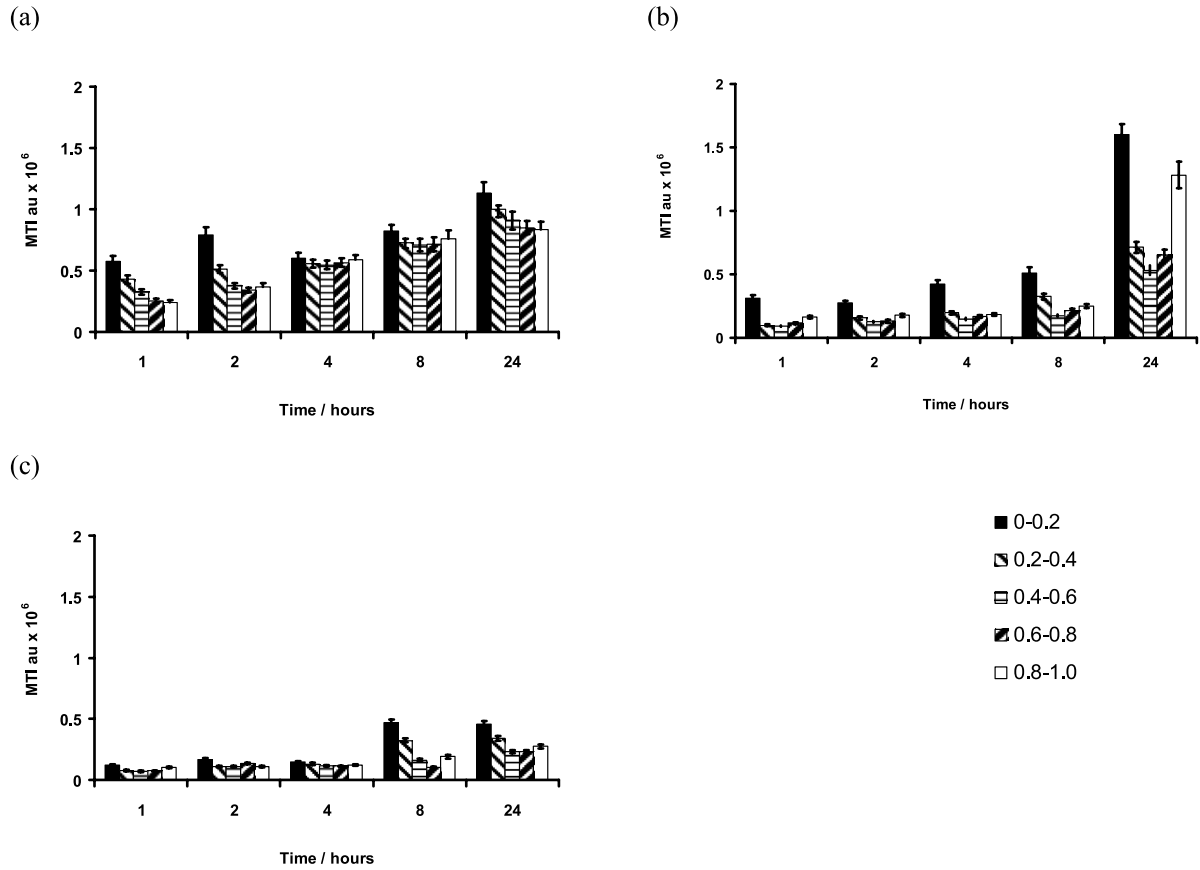


Fig. 9. Histograms illustrating the average MTI of FITC-dextran in five equal sections of the 3 mm thick agarose constructs in the confined bioreactor at a mean flow velocity of 1.27 mm/h. Molecules of size (a) 4 kDa (FD-4), (b) 500 kDa (FD-500) and (c) 2,000 kDa (FD-2000). Data represents mean \pm standard deviation of 4–6 replicates.

within the confined bioreactor was not conducive to molecular transport. Therefore, any subsequent enhancement may be solely attributed to the fluid convection.

As with the diffusion samples, fluorescence accumulating within the perfused constructs was inversely related to the molecular weight of the dextran (Figs 9 and 10). Figure 10a demonstrates that for the entire construct, the perfusion of FD-4 increases monotonically over the 24 h. At all time points, the total fluorescence for FD-4 molecules were higher than the corresponding values for FD-500 and FD-2000 within the 3 mm thick constructs (Fig. 10b and c, respectively).

The percentage difference in t MTI values between the perfused and diffusion experiments were estimated using the following equation:

$$\left(\frac{P - F_S}{F_S} \right) * 100\%, \quad (5)$$

where P and F_S are the fluorescent values associated with perfusion and diffusion, respectively. Values for both the complete construct and their central core are summarized in Table 3 for each time point. The data indicate that the increased dextran FD-4 concentration by perfusion was initially high. The highest percentage values corresponded to FD-4 fluorescence in the whole construct at 1 and 2 h, during which

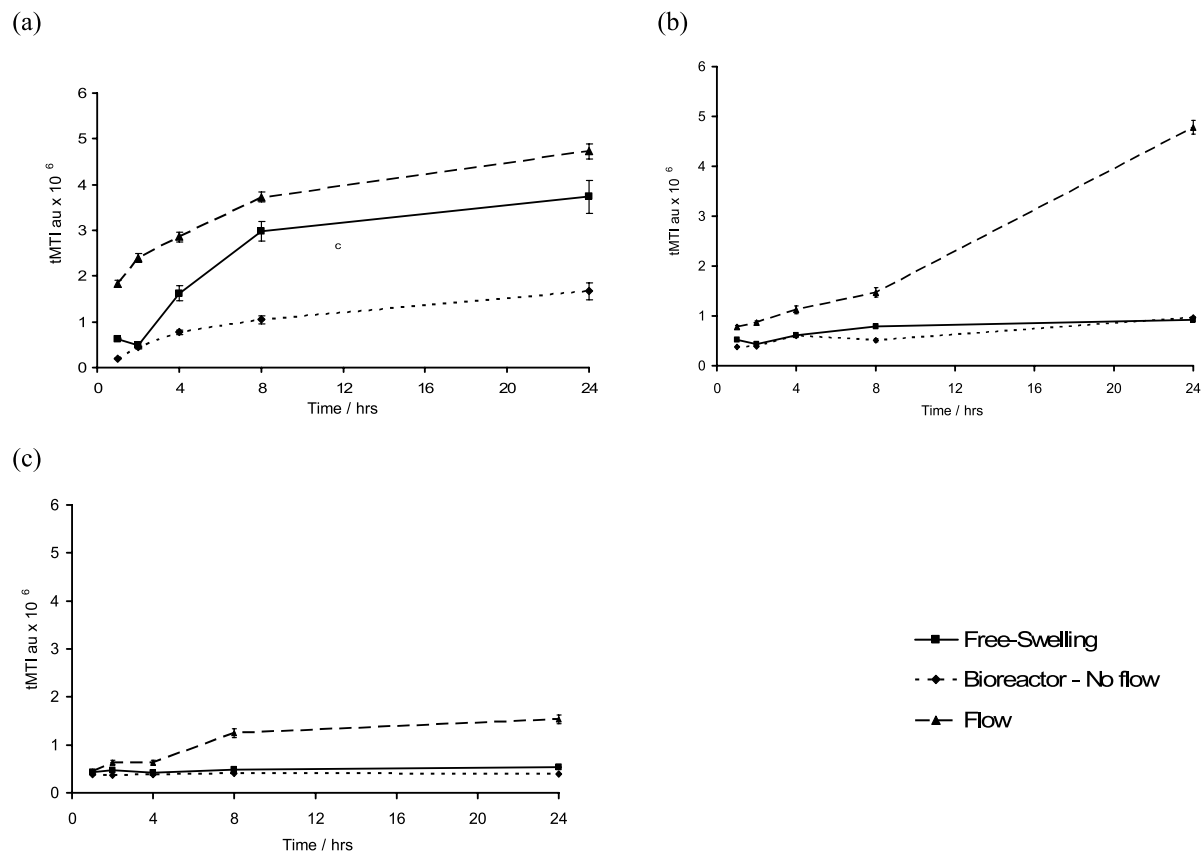


Fig. 10. Graphs demonstrating the influence of perfusion on the total mass transport index ($tMTI$) of dextran molecules (a) FD-4, (b) FD-500 and (c) FD-2000 that had entered the construct over the 24 h period. The fluorescence is presented as arbitrary units (au) and the error bars correspond to the standard deviation of 4–6 replicates.

Table 3

Total mass transport indices of dextran molecules perfused using the perfusion bioreactor

Time (h)	$tMTI$ -% change between perfusion and free-swelling					
	Whole construct			Central region		
	FD-4	FD-500	FD-2000	FD-4	FD-500	FD-2000
1	192	104	19	242	29	1
2	388	125	73	359	82	56
4	76	87	63	132	95	63
8	25	188	203	21	110	121
24	27	395	294	30	291	222

Note: The data represent percentage change to fluorescent values, which were obtained by comparing the perfusion values to their free-swelling values within the complete construct and at the central region of interest.

period, the percentage increases were approximately 192% and 388%, respectively. The corresponding increase in the central region after 1 and 2 h was 242% and 359%, respectively. At 24 h, however, the corresponding enhancement of dextran FD-4 by perfusion had decreased to 27% at the construct centre, and to 30% globally. By contrast, the larger sized dextran molecules, FD-500 and FD-2000 generally increased steadily over the 24 h period. Moreover, by 8 h, the influence of perfusion on their accumulation at the central region had exceeded that of the FD-4 molecules. By 24 h, the increased molecular concentration within the constructs and at the centre was greatest for FD-500: an increase of 395% for the complete construct and 291% for the central region.

3.3. Influence of media perfusion on DNA and GAG production

The temporal profiles of DNA concentrations per unit construct mass, for both the complete constructs and their central core region are presented in Fig. 11. The DNA concentrations were similar at day 1 for both the free-swelling and perfused cultures. The 24 h values were 172.2 and 169.1 $\mu\text{g/g}$ of constructs for the free-swelling and perfused constructs, respectively. These rose by 48% at day 20 for the free-swelling culture, while, the perfused culture increased by 75%. In the central cores of the agarose constructs, the 24 h DNA appeared unaffected by media perfusion. A difference between the free-swelling and

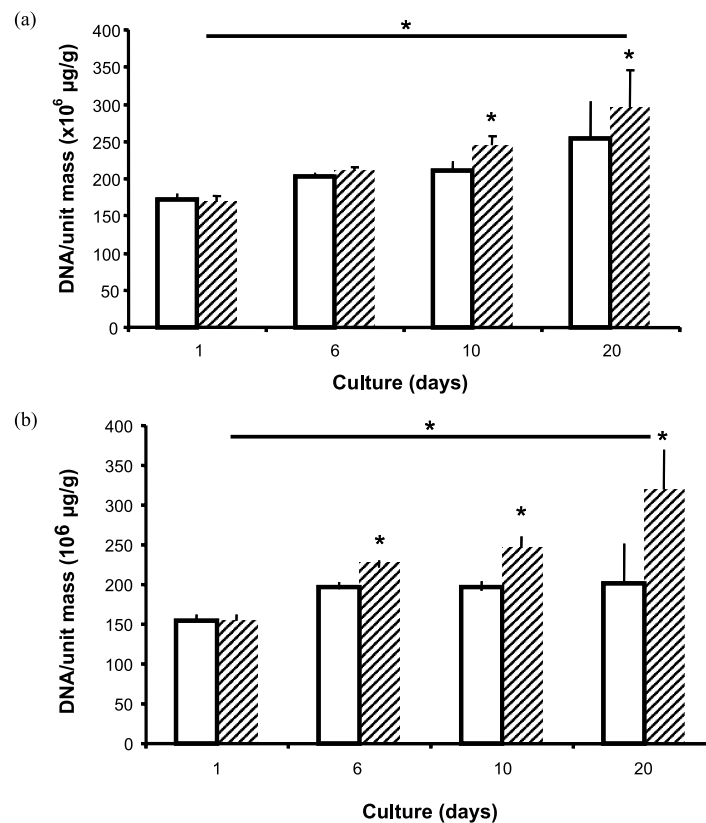


Fig. 11. DNA concentrations within (a) the complete construct and (b) the central region over the 20 day culture period. The white boxes represent the free-swelling cultures, while the shaded boxes represent the perfused cultures (mean \pm standard deviation, $n = 9$ samples). * represents statistical significance ($p < 0.05$, ascertained by Students t -test) between perfusion and free-swelling cultures.

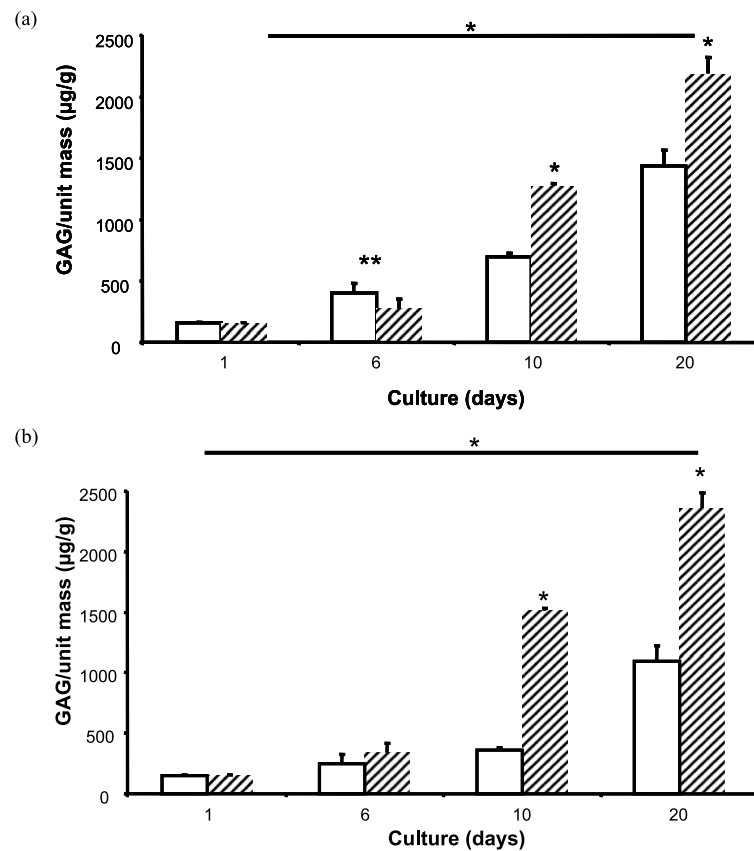


Fig. 12. GAG concentrations within (a) the complete construct and (b) the central region over the 20 day culture period. The white boxes represent the free-swelling cultures, while the shaded boxes represent the perfused cultures (mean \pm standard deviation, $n = 9$ samples). * represents statistical significance ($p < 0.05$, ascertained by Students t -test) between perfusion and free-swelling cultures. ** denotes a time point whereby GAG accumulation by the articular chondrocytes was higher in the free-swelling than the perfused cultures.

perfused cultures was first observed at day 6, and was most pronounced at day 20. By this time, the DNA concentrations had only risen by 30% for the free-swelling culture, while there was 106% increase in the perfused culture. The latter represented the highest difference observed between the experimental and the control groups.

Concentrations of sulphated GAG within the cultured constructs (Fig. 12) were not significantly different in the free-swelling and perfused constructs at 24 h. At day 6, constructs cultured under the free-swelling conditions had higher GAG concentration than those cultured in the perfusion bioreactor. By day 10 and onwards, the perfusion bioreactor enhanced GAG content was comparable to that in the free-swelling constructs. Thus, the GAG concentration over 20 days for the whole constructs increased from the day 1 values by approximately 8 and 13 times in free-swelling and perfused cultures, respectively. The most significant difference between the two cultures occurred at their central cores (Fig. 12b). As with the whole constructs, the day 1 values were similar in both cultures, and the day 6 GAG production was marginally higher in the perfused culture. However, by day 10, the GAG concentration at the centre of the free-swelling cultures, had fallen to approximately 49% of the average value for the

whole constructs, and to 24% at day 20. By contrast, the average GAG concentration at the centre of the perfused constructs had risen by approximately 19% at day 10 and by 8% at day 20.

4. Discussion

The aims of the present study were to describe the design of the perfusion bioreactor, its effectiveness in transporting large molecules through diffusion-starved hydrogels, and in turn, the effects on the cells cultured therein.

The use of perfusion bioreactors is not new in tissue engineering. However, different rationales have driven their designs. For example, the design by Wendt and co-workers [47] primarily perfused cells through and around their scaffold, with the aim of achieving an initial homogeneous distribution of cells through out the scaffold. Démarteau et al. [7] mechanically deformed the cell-seeded constructs, while the bioreactor from Neves and colleagues [32] perfused culture media through and around the constructs. In contrast, the present study focused on molecular transport, which, for cells within 3D constructs means nutrient delivery. This, therefore, influenced the model system used, and ultimately the design features of the bioreactor. For example, in order to envisage nutritional demand throughout the cell-seeded constructs, there had to be cellular homogeneity. The most effective method of achieving this was to use a hydrogel scaffold. To this end, the cells were mixed while the agarose was molten, ensuring homogeneity, and then cast into the appropriate mould (CP₂), and allowed to set. The hydrogel presented the additional advantage of having physicochemical properties (pore size 364 ± 8 nm to 201 ± 4 nm in gel concentrations of 2% and 5%, respectively [34]), closer to that of native cartilage, than the microporous scaffold used in other studies. Additionally, in order to effectively transport molecules to the centre of the constructs, fluid flow around its edges had to be eliminated. Given that a perfused fluid will always travel the path of least resistance, it is clear that when care is not taken, the fluid will flow around and not through the construct. By threading the inner wall of CP₂, and allowing the cell-seeded agarose to set therein, the construct therefore is mechanically locked inside CP₂, and lateral flow is prevented. Such mechanical locking of cellular constructs to a flow chamber is necessary, and has not been previously demonstrated.

The higher fluorescence associated with the FD-4 experiments compared to FD-500 and FD-2000 was attributed to its higher diffusivity. Ljunglof and Thommes [27] observed a similar trend with respect to the concentration gradient of molecules diffusing from the surface, to the central core of cartilage discs. This spatial concentration gradient declined with time, such that the molecular concentrations at the core began to equilibrate with the surface concentration after 2 h incubation. In the present study, however, diffusion did not yield equilibrium within the 24 h for any of the three different sized dextran molecules. In the studies of Ljunglof and Thommes [27], their attainment of a homogeneous concentration within a short length of time could be explained by the relatively low diffusion distance of 100 μ m.

The FITC-dextran used in the present study had molecular weights of 4, 500 and 2,000 kDa. These sizes are comparable to those of the growth factor IGF1 (7.7 kDa), an aggrecan molecule (210 kDa, approximately half the size of FD-500), or an aggregate of aggrecan molecules complex (2,600 kDa). The diffusive transport of small molecules such as glucose and oxygen within intervertebral discs has been observed to be sufficient for cellular requirements [18,30,43,44]. In fact, subtle differences have been observed between the diffusive and convective transport of dextran 400 Da molecules [10]. Nevertheless, researchers have shown that the transport of glucose in tissue-engineered constructs is hindered during prolonged culture, due to the high activity of cells at the peripheral region, making cell growth and neo-tissue development at the centre is unsustainable [17,31]. Thus, the present study aimed to enhance

transport of both small and large-sized molecules by perfusion. In this regard, higher fluorescent intensities were observed within the perfused constructs, compared to the diffusion constructs. Moreover, this was made clear for FD-2000 molecules after 8 h (Fig. 9). The large molecules, which had hardly *diffused* were greatly aided by the convecting fluid (Fig. 7c). By 24 h, its transportation by perfusion was 3 times higher than by diffusion at the peripheral margins, and twice the value by diffusion at the central core (Table 3).

The conformation of the dextrans is linear, such that their differences in diffusivity are directly related to their chain length. The influence of chain length on dextran diffusivity is comparable to the influence of number of base pairs to the diffusion coefficient of DNA in gels [24], and is given by:

$$D_G = 0.196 \frac{k_B T}{\eta R_H} \approx N_0^{-1/2}, \quad (6)$$

where D_G is the diffusion coefficient in gels, k_B is the Boltzman constant, T is the absolute temperature, η is the medium viscosity, and R_H and N_0 are the chain radius and the number of base pairs, respectively. It is evident that an inverse relationship exists between the diffusivity of a DNA molecule and the number of its base pairs. Hence, it is deducible that the diffusivity of unbranched macromolecules, such as dextran, is inversely proportional to their chain length, which is directly related to its size. Indeed, this size-dependence of dextran diffusivity has previously been observed by Pluen et al. [35], using different sized FITC-dextran and agarose gels.

Although perfusion increased the dextran concentration within the agarose constructs, a homogeneous distribution of dextran molecules was not achieved within the experimental period. This depth-dependence is comparable to the temporal decrease of molecular diffusivity within porous materials described by Clark et al. [5]. The authors modelled the declining diffusivity of enzymes due to a reduction in the effective pore cross-section resulting from the adsorption of molecules onto pore surfaces and accumulation in the pore walls. The reduced effective pore area, which ultimately causes the decline of permeability, is suggested to increase with respect to both experimental period and molecular weight of the diffusing particle [16]. Therefore, it is possible that micropores close to the periphery of the constructs may become blocked by dextran chains early in the experiments and restrict subsequent transport of dextran molecules to the construct core. Consequently, the difference in dextran concentration between the periphery and the central core of the constructs may increase with perfusion time.

The results of the DNA and GAG measurements within the papain-digested chondrocyte/agarose constructs indicated that the concentration of both molecules generally increased with culture time. The average increase in DNA and GAG by the bioreactor was 75% and 1340%, respectively for the complete constructs, while at their centre, the DNA and GAG increased by 106% and 1603%, respectively after 20 days culture. The slower increase of DNA concentration at the centre of the free-swelling constructs is in good agreement with previous studies, as indeed is its severity with prolonged culture [17,31]. This decline of viable cell concentration at the centre has been proposed to result from either an insufficient supply of soluble nutrients to cells at the centre or an inadequate cell concentration at the centre to stimulate cellular functions [11,18]. The latter explanation is more applicable to macroporous scaffolds, such as PGA and PLLA, where, heterogeneous seeding densities are common. However, in the present work, the cells were added to the agarose in a molten state. The suspension was mixed and allowed to set in the desired mould. Therefore, the initial cell concentration of 20×10^6 cells/ml was homogeneous throughout the constructs. In addition, the high cellular viability at the construct periphery suggests that this cell concentration is sufficient to support cellular function. Therefore, nutrient deprivation at the construct centre is most likely the cause of the reduced cell concentration.

The physiological content of GAG within articular cartilage is between 4% and 7% [46], while the DNA concentration is approximately 0.66% [12] depending on depth from the articular surface. Although media perfusion resulted in neither a physiological concentration of DNA nor of GAG within the constructs, a significant enhancement over free-swelling culture was achieved globally and at the central core, over the 20 days of culture.

The bioreactor designed in this study enabled small and large molecules to be transported into the agarose cylinders. Using fluorescence-labelled molecules, the distributions of the diffused and perfused molecules were visualized across the thickness of the constructs. We have been able to demonstrate an enhanced transportation of different-sized molecules by perfusion. Moreover, for FD-2000 molecules, perfusion was the sole means of transport. We also demonstrated that although a homogeneous distribution of molecules could not be achieved by perfusion within 24 h, the enhancement at the cores of the constructs, results in significant improvements to cellular proliferation and matrix production during prolonged culture.

This study therefore provides a platform that may lead to combating the nutrient deficiency at the centre of 3D tissue-engineered constructs.

Acknowledgement

The work was funded by the Engineering and Physical Sciences Research Council, UK (EPSRC).

References

- [1] G.H. Altman, H.H. Lu, R.L. Horan et al., Advanced bioreactor with controlled application of multi-dimensional strain for tissue engineering, *J. Biomech. Eng.* **124** (2002), 742–749.
- [2] M.A. Anderson, J.T. Payne, J.M. Kreeger et al., Effects of intra-articular chlorhexidine diacetate lavage on the stifle in healthy dogs, *Am. J. Vet. Res.* **54** (1993), 1784–1789.
- [3] M. Brittberg, A. Lindahl, A. Nilsson et al., Treatment of deep cartilage defects in the knee with autologous chondrocyte transplantation, *N. Engl. J. Med.* **331** (1994), 889–895.
- [4] C.A. Chung, C.W. Yang and C.W. Chen, Analysis of cell growth and diffusion in a scaffold for cartilage tissue engineering, *Biotech. Bioeng.* **94** (2006), 1138–1146.
- [5] D.S. Clark, J.E. Bailey and D.D. Do, A mathematical-model for restricted diffusion effects on macromolecule impregnation in porous supports, *Biotech. Bioeng.* **27** (1985), 208–213.
- [6] T. Davisson, R.L. Sah and A. Ratcliffe, Perfusion increases cell content and matrix synthesis in chondrocyte three-dimensional cultures, *Tissue Eng.* **8** (2002), 807–816.
- [7] O. Demartean, M. Jakob, D. Schafer et al., Development and validation of a bioreactor for physical stimulation of engineered cartilage, *Biorheology* **40** (2003), 331–336.
- [8] S. Falsafi and R.J. Koch, Growth of tissue-engineered human nasoseptal cartilage in simulated microgravity, *Arch. Otolaryngol. Head Neck Surg.* **126** (2000), 759–765.
- [9] R.W. Farndale, C.A. Sayers and A.J. Barrett, A direct spectrophotometric microassay for sulfated glycosaminoglycans in cartilage cultures, *Connect. Tissue Res.* **9** (1982), 247–248.
- [10] S.J. Ferguson, K. Ito and L.P. Nolte, Fluid flow and convective transport of solutes within the intervertebral disc, *J. Biomech.* **37** (2004), 213–221.
- [11] L.E. Freed, A.P. Hollander, I. Martin et al., Chondrogenesis in a cell-polymer-bioreactor system, *Exp. Cell Res.* **240** (1998), 58–65.
- [12] L.E. Freed, J.C. Marquis, A. Nohria et al., Neocartilage formation *in vitro* and *in vivo* using cells cultured on synthetic biodegradable polymers, *J. Biomed. Mater. Res.* **27** (1993), 11–23.
- [13] L.E. Freed, G. Vunjak-Novakovic, R.J. Biron et al., Biodegradable polymer scaffolds for tissue engineering, *Biotechnology (NY)*, **12** (1994), 689–693.
- [14] G.K. Gorti, J. Lo, S. Falsafi et al., Cartilage tissue engineering using cryogenic chondrocytes, *Arch. Otolaryngol. Head Neck Surg.* **129** (2003), 889–893.

- [15] D.A. Grande, C. Halberstadt, G. Naughton et al., Evaluation of matrix scaffolds for tissue engineering of articular cartilage grafts, *J. Biomed. Mater. Res.* **34** (1997), 211–220.
- [16] J. Gutenwik, B. Nilsson and A. Axelsson, Effect of hindered diffusion on the adsorption of proteins in agarose gel using a pore model, *J. Chromatogr. A* **1048** (2004), 161–172.
- [17] H.K. Heywood, P.K. Sembi, D.A. Lee and D.L. Bader, Cellular utilization determines viability and matrix distribution profiles in chondrocyte-seeded alginate constructs, *Tissue Eng.* **10** (2004), 1467–1479.
- [18] S. Holm, A. Maroudas, J.P. Urban et al., Nutrition of the intervertebral disc: solute transport and metabolism, *Connect. Tissue Res.* **8** (1981), 101–119.
- [19] E.B. Hunziker, Biologic repair of articular cartilage. Defect models in experimental animals and matrix requirements, *Clin. Orthop. Relat. Res.* **367**(Suppl.) (1999), S135–S146.
- [20] D.W. Hutmacher, Scaffolds in tissue engineering bone and cartilage, *Biomaterials* **21** (2000), 2529–2543.
- [21] S.L. Ishaug, G.M. Crane, M.J. Miller et al., Bone formation by three-dimensional stromal osteoblast culture in biodegradable polymer scaffolds, *J. Biomed. Mater. Res.* **36** (1997), 17–28.
- [22] W. Kafienah, M. Jakob, O. Demarteau et al., Three-dimensional tissue engineering of hyaline cartilage: comparison of adult nasal and articular chondrocytes, *Tissue Eng.* **8** (2002), 817–826.
- [23] Y.J. Kim, R.L. Sah, J.Y. Doong and A.J. Grodzinsky, Fluorometric assay of DNA in cartilage explants using Hoechst 33258, *Anal. Biochem.* **174** (1988), 168–176.
- [24] W. Kuhn, Concerning the shape of thread shapes molecules in solution, *Kolloid-Zeitschrift* **68** (1934), 2–15.
- [25] M.C. Lewis, B.D. Macarthur, J. Malda et al., Heterogeneous proliferation within engineered cartilaginous tissue: the role of oxygen tension, *Biotech. Bioeng.* **91** (2005), 607–615.
- [26] P.J. Livesley, M. Doherty, M. Needoff and A. Moulton, Arthroscopic lavage of osteoarthritic knees, *J. Bone Joint Surg. Br.* **73** (1991), 922–926.
- [27] A. Ljunglof and J. Thommes, Visualising intraparticle protein transport in porous adsorbents by confocal microscopy, *J. Chromatogr. A* **813** (1998), 387–395.
- [28] J. Malda, J. Rouwkema, D.E. Martens et al., Oxygen gradients in tissue-engineered PEGT/PBT cartilaginous constructs: measurement and modeling, *Biotech. Bioeng.* **86** (2004), 9–18.
- [29] D. Marolt, A. Augst, L.E. Freed et al., Bone and cartilage tissue constructs grown using human bone marrow stromal cells, silk scaffolds and rotating bioreactors, *Biomaterials* **27** (2006), 6138–6149.
- [30] A. Maroudas, Transport of solutes through cartilage: permeability to large molecules, *J. Anat.* **122** (1976), 335–347.
- [31] I. Martin, B. Obradovic, L.E. Freed and G. Vunjak-Novakovic, Method for quantitative analysis of glycosaminoglycan distribution in cultured natural and engineered cartilage, *Ann. Biomed. Eng.* **27** (1999), 656–662.
- [32] A.A. Neves, N. Medcalf and K. Brindle, Functional assessment of tissue-engineered meniscal cartilage by magnetic resonance imaging and spectroscopy, *Tissue Eng.* **9** (2003), 51–62.
- [33] D. Pazzano, K.A. Mercier, J.M. Moran et al., Comparison of chondrogenesis in static and perfused bioreactor culture, *Biotech. Progr.* **16** (2000), 893–896.
- [34] N. Pernodet, M. Maaloum and B. Tinland, Pore size of agarose gels by atomic force microscopy, *Electrophoresis* **18** (1997), 55–58.
- [35] A. Pluen, P.A. Netti, R.K. Jain and D.A. Berk, Diffusion of macromolecules in agarose gels: comparison of linear and globular configurations, *Biophys. J.* **77** (1999), 542–552.
- [36] M. Steinwachs and P.C. Kreuz, Autologous chondrocyte implantation in chondral defects of the knee with a type I/III collagen membrane: a prospective study with a 3-year follow-up, *Arthroscopy* **23** (2007), 381–387.
- [37] K.R. Stone, A.W. Walgenbach, A. Freyer et al., Articular cartilage paste grafting to full-thickness articular cartilage knee joint lesions: a 2- to 12-year follow-up, *Arthroscopy* **22** (2006), 291–299.
- [38] P. Sucusky, D.F. Osorio, J.B. Brown and G.P. Neitzel, Fluid mechanics of a spinner-flask bioreactor, *Biotech. Bioeng.* **85** (2004), 34–46.
- [39] R. Sutherland, J. Freyer, W. Mueller-Klieser et al., Cellular growth and metabolic adaptations to nutrient stress environments in tumor microregions, *Int. J. Radiat. Oncol. Biol. Phys.* **12** (1986), 611–615.
- [40] T. Tallheden, C. Bengtsson, C. Brantsing et al., Proliferation and differentiation potential of chondrocytes from osteoarthritic patients, *Arthritis Res. Ther.* **7** (2005), R560–R568.
- [41] S.R. Tew, A.P. Kwan, A. Hann et al., The reactions of articular cartilage to experimental wounding: role of apoptosis, *Arthritis Rheum.* **43** (2000), 215–225.
- [42] B.R. Unsworth and P.I. Lelkes, Growing tissues in microgravity, *Nat. Med.* **4** (1998), 901–907.
- [43] J.P. Urban, S. Holm, A. Maroudas and A. Nachemson, Nutrition of the intervertebral disk. An *in vivo* study of solute transport, *Clin. Orthop. Relat. Res.* **129** (1977), 101–114.
- [44] J.P. Urban, S. Holm, A. Maroudas and A. Nachemson, Nutrition of the intervertebral disc: effect of fluid flow on solute transport, *Clin. Orthop. Relat. Res.* **170** (1982), 296–302.
- [45] N. Veilleux and M. Spector, Effects of FGF-2 and IGF-1 on adult canine articular chondrocytes in type II collagen-glycosaminoglycan scaffolds *in vitro*, *Osteoarthr. Cartil.* **13** (2005), 278–286.

- [46] G. Vunjak-Novakovic, I. Martin, B. Obradovic et al., Bioreactor cultivation conditions modulate the composition and mechanical properties of tissue-engineered cartilage, *J. Orthop. Res.* **17** (1999), 130–138.
- [47] D. Wendt, A. Marsano, M. Jakob et al., Oscillating perfusion of cell suspensions through three-dimensional scaffolds enhances cell seeding efficiency and uniformity, *Biotech. Bioeng.* **84** (2003), 205–214.
- [48] X. Xu, J.P. Urban, U. Tirlapur et al., Influence of perfusion on metabolism and matrix production by bovine articular chondrocytes in hydrogel scaffolds, *Biotech. Bioeng.* **93** (2006), 1103–1111.